High pressure x-ray diffraction study of the volume collapse in Ba24Si100 clathrate

Pierre Toulemonde, D. Machon, A. San Miguel, M. Amboage

High pressure x-ray diffraction study of the volume collapse in $Ba_{24}Si_{100}$ clathrate

P. Toulemonde*
Institut Néel, CNRS and Université Joseph Fourier, 25 avenue des Martyrs, BP 166, F-38042 Grenoble Cedex 9, France

D. Machon and A. San Miguel
Université de Lyon, Laboratoire PMCN, CNRS, UMR 5586, Université Lyon 1, Villeurbanne 69622, France

M. Amboage
ESRF, B.P. 220, 6 rue Jules Horowitz, F-38043 Grenoble, France and Diamond Light Source Ltd., Harwell Science and Innovation Campus, Didcot, Oxfordshire OX11 0DE, United Kingdom

(Received 24 September 2010; revised manuscript received 25 February 2011; published 8 April 2011)

The high pressure stability of the silicon type-III clathrate $Ba_{24}Si_{100}$ has been studied by x-ray diffraction (XRD) up to a maximum pressure of 37.4 GPa. The high pressure behavior of this Si type-III clathrate appears to be analogous to the structural type-I parent Ba_8Si_{46}. An isostructural volume collapse is observed at ~23 GPa, a value higher than for Ba_8Si_{46} (13–15 GPa). The crystallinity of the structure is preserved up to the maximum attained pressure without amorphization, which appears to be in contradiction with the interpretation given in a Raman spectroscopy study [Shimizu *et al.*, Phys. Rev. B **71**, 094108 (2005)]. Nevertheless, the XRD analysis shows the appearance of a type-III disordered nanocaged-based crystalline structure after the volume collapse. Moreover, we find that the volume collapse transformation is (quasi)reversible after pressure release. Additionally, a low pressure transition first evidenced by Raman spectroscopy is also observed in our XRD study at 5 GPa: The variation of the isotropic thermal factors of Ba atoms shows a clear discontinuity at this pressure while the average positions of Ba atoms remain identical.

DOI: 10.1103/PhysRevB.83.134110 PACS number(s): 61.50.Ks, 82.75.Fq, 62.50.−p

I. INTRODUCTION

Inorganic clathrates based on group IV elements (C, Si, Ge, Sn) have attracted a renewed interest in the past years since their discovery in the 1960s.[1,2] Indeed, due to their crystallographic structure based on nanocages (with 20, 24, or 28 atoms) more or less filled by guest atoms, their physical properties can be tuned,[3,4] making such a class of materials interesting for potential technological applications in electronics, optics, or mechanics. One way to explore their properties is to use pressure as a thermodynamic variable which allows to continuously modify the interaction between the host and the guest substructures. This methodology has been followed by different scientific groups in the past decade for clathrate systems. Only very few studies on type-III clathrates under high pressure have been conducted. Grosche *et al.* have studied the superconducting behavior of type-III $Ba_{24}Ge_{100}$ and $(Ba_4Na_2)Ge_{100}$ germanium-based clathrates up to 3.4 GPa and in low temperature[5–7] while Shimizu *et al.* have reported a Raman spectroscopy study of $Ba_{24}Ge_{100}$ up to 26 GPa at room temperature.[8] Two published works report on the high pressure behavior of $Ba_{24}Si_{100}$, the compound studied in the present article: a low temperature resistivity study up to 1.15 GPa (Ref. 9) of its superconducting regime and a Raman spectroscopy study by Shimizu *et al.* at room temperature up to 27 GPa.[10] To the best of our knowledge, no high pressure x-ray diffraction study of $Ba_{24}Si_{100}$ has been published. Let us turn to type-I silicon-based clathrates, which are structurally related, simpler, and more documented both experimentally and theoretically. In the Ba_8Si_{46} type-I clathrate,[11] it is now well established that a volume collapse takes place at pressures of 13–15 GPa.[3,12,13] This unusual second-order transition is more precisely an isostructural homothetic volume collapse (HVC), i.e., the full structure is preserved through the transition, with the relative atomic positions remaining the same during the whole process.[14,15] This HVC seems to be a general trend in type-I silicon clathrates (built on Si_{20} and Si_{24} cages): It is observed in heavy alkaline-doped Si clathrates [K_8Si_{46} (Refs. 16 and 17), Rb_6Si_{46} (Ref. 18)], in alkaline-earth intercalated Si clathrates [Ba_8Si_{46}, $(Ba_6Sr_2)Si_{46}$, $Ba_8(Si_{40}Ag_6)$],[3,19,20] and in the halogen-doped clathrate $I_8(Si_{44}I_2)$.[3,21] In type-II silicon clathrates (i.e., M_xSi_{136} with M = Na, for example) the silicon network (made of Si_{20} and Si_{28} cages) evolves discontinuously (first-order transition) toward the β-tin structure at 10–11 GPa (Refs. 12 and 22) (see Fig. 5 below). Is this HVC scheme also valid in the analogous $Ba_{24}Si_{100}$ type-III clathrate?[23,24] Type-III clathrates are built from the same silicon-based Si_{20} cages as in Ba_8Si_{46} and from distorted Si_{20} (in fact, the same Si_{24} cages of those from Ba_8Si_{46} with four vacancies of Si), also giving rise to cubic Si_8 cages (see Fig. 1).

The high pressure (HP) Raman spectroscopy study of $Ba_{24}Si_{100}$ by Shimizu *et al.*[10] has evidenced two transitions. The first one, between 3.9 and 6.5 GPa, is characterized by the splitting of the 126 cm^{-1} Raman mode and a general decrease of the intensity of the modes associated with the vibrations of Ba atoms. The second one, at 20.7–23.2 GPa, is associated with the disappearance of all the Raman modes, which was attributed to a pressure-induced amorphization by the authors of that work. In Ba_8Si_{46}, the pressure evolution of the Raman signal shows some similitudes: At ~7 GPa the lowest-frequency modes disappear, then at the HVC at ~13–15 GPa, the Raman spectrum is drastically affected, showing six large bands above the HVC, and finally the Bragg

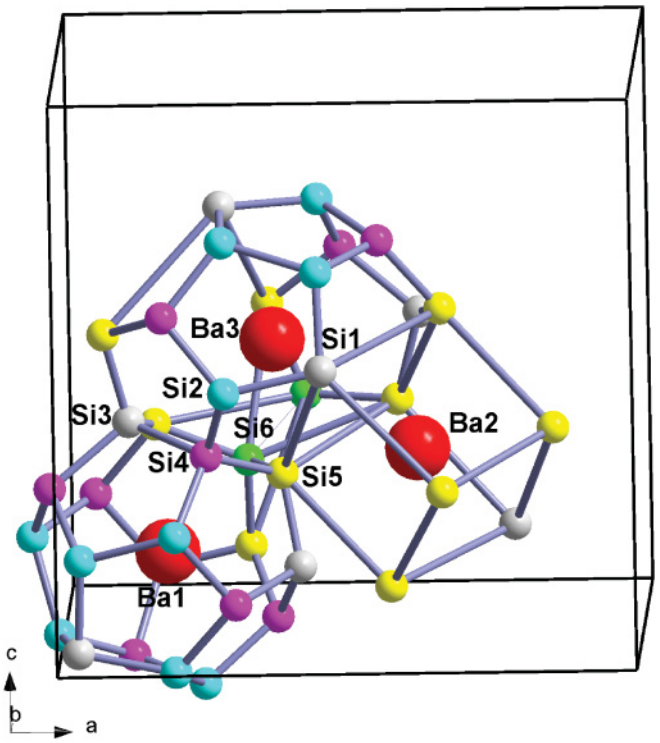

FIG. 1. (Color online) Partial crystallographic structure of $Ba_{24}Si_{100}$ showing the different cages around the three Ba sites and the corresponding Si sites forming the Si network [see the text for a description of Si(1), Si(2), Si(3), Si(4), Si(5), Si(6) and Ba(1), Ba(2), Ba(3) sites].

peaks of its x-ray diffraction (XRD) pattern disappear above 40 GPa, proof that Ba_8Si_{46} becomes irreversibly amorphous at higher pressure.

In Ba_8Si_{46} the nature of the first transition at 7 GPa is related to a change of the hybridization of Ba orbitals with Si orbitals, accompanied with a charge transfer from Ba in the small Si_{20} cages toward the Si framework. The induced change of the polarizability of Ba in the large Si_{24} cage shown by HP Raman scattering,[13] the jump ~5 GPa in the x-ray absorption near-edge structure (XANES) L_3 absorption edge of Ba (Ref. 15), and a recent analysis of HP XRD patterns by the maximum entropy method[25] support this scenario. Another scenario related to an off-centering of Ba in large Si_{24} cages could explain the first transition occurring at 5–7 GPa in Ba_8Si_{46}, but from extended x-ray-absorption fine structure (EXAFS) experiments performed at the Ba K edge on Ba_8Si_{46}, we can exclude it, within the error bar of the EXAFS analysis, which is ~0.3 Å (Refs. 15 and 26) in those measurements. In $Ba_{24}Si_{100}$, the second transition observed by HP Raman spectroscopy at ~22–23 GPa was interpreted as a sign of amorphization, because of the irreversible loss of all Raman-active modes above this pressure.

In this paper we show by *in situ* XRD that the transition at 23 GPa does not correspond to the amorphization of the $Ba_{24}Si_{100}$ clathrate but to the volume collapse transition. In addition, our high pressure excursion shows that the transition is reversible, at least up to 37 GPa.

II. EXPERIMENTAL

The $Ba_{24}Si_{100}$ sample was synthesized in a high pressure belt-type apparatus, as reported elsewhere.[20,24] We started with commercial $BaSi_2$ (CERAC, 98%) and Si (Alfa, 99.9%) powders. Both precursors were mixed together and grind in the nominal ratio. The mixture was compacted in small cylindric pellets (4 mm diam and 5 mm length) and placed into a closed hexagonal boron nitride crucible. The entire assembly was introduced inside the carbon tube heater inserted in the pyrophyllite HP gasket. The temperature was previously calibrated using a chromel-alumel thermocouple. The HP-HT synthesis was performed at 1.1 GPa and 650 °C. The pressure was first increased up to 1.1 GPa, then the sample was slowly heated up to 650 °C and maintained at this temperature for 1 h, and then quenched rapidly to room temperature. Finally the pressure was released to room pressure and the sample recovered.

XRD patterns were collected using a Siemens D-500 powder diffractometer working in the Bragg-Brentano geometry at a wavelength $\lambda_{Cu,K\alpha_{1,2}} = 1.5418$ Å from $2\theta = 10°$ to 120° in steps of 0.02°.

A Raman spectrum was also recorded at room temperature using a Jobin-Yvon HR-800 Labram spectrometer double-notch filtering and air-cooled CCD detector. The measurement was performed without heating or damaging the sample by using an adapted power of an excitation laser with a wavelength of 514 nm.

The HP *in situ* synchrotron XRD experiment was carried out using a He gas membrane-driven diamond-anvil cell (DAC) with diamonds having a culet size of 350 μm. Samples were loaded using nitrogen as a pressure-transmitting medium, and the pressures were determined using the ruby fluorescence method. Pressure was increased by small steps of 0.5–1 GPa and the system was left to equilibrate for 15–30 min at each pressure. Synchrotron radiation measurements were performed at the ID9A beamline of the European Synchrotron Radiation Facility via angle-dispersive diffraction techniques using monochromatic radiation $\lambda = 0.4108$ Å. Diffraction patterns were collected using image plate detection. The sample-to-detector distance and the image plate orientation angles were calibrated using a polycrystalline powder Si standard. The two-dimensional diffraction images were analyzed using the FIT2D software,[27] yielding one-dimensional intensity versus diffraction angle 2θ patterns.

III. RESULTS AND DISCUSSION

A. Ambient pressure characterization of the $Ba_{24}Si_{100}$ sample

Figure 2 shows the XRD pattern and the Raman spectrum (inset of Fig. 2) of our polycrystalline $Ba_{24}Si_{100}$ sample obtained at ambient conditions. Both are in good agreement with the ones published in previous works.[10,23,24] The XRD pattern shows that the sample is nearly single phase and contains traces of remaining Si and cubic $BaSi_2$ phases (their main Bragg peaks indicated an overlap with the reflections of $Ba_{24}Si_{100}$). The cubic lattice parameter refined from this XRD pattern at ambient pressure [$a = 14.061(1)$ Å] is in agreement with those already reported.[23,24]

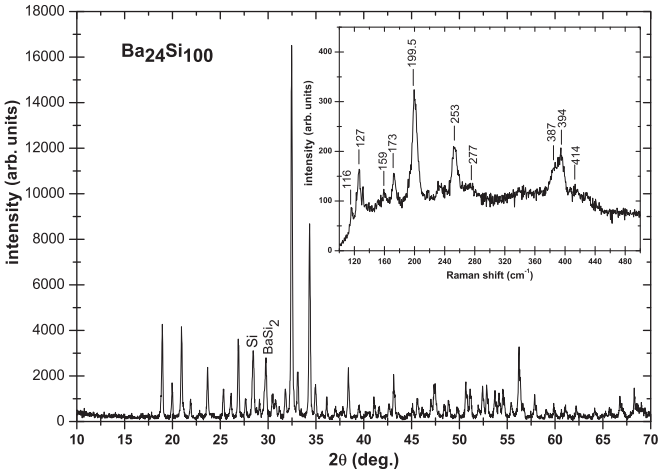

FIG. 2. XRD pattern ($\lambda = 1.5418$ Å) of our $Ba_{24}Si_{100}$ powder sample and Raman spectrum (inset) at ambient pressure and room temperature; the main Bragg peaks of Si and $BaSi_2$ impurities are indicated; ticks in the inset show the main active Raman modes

B. Description of the method based on Rietveld refinements used for the XRD patterns analysis

The structural parameters of $Ba_{24}Si_{100}$ were refined from XRD patterns by the Rietveld method using the software FULLPROF.[28] Data points within the range $1.90^\circ < 2\theta < 24^\circ$ were taken into account. The profile shape was calculated based on a pseudo-Voigt function. The background was fitted using a linear interpolation between points.

The $Ba_{24}Si_{100}$ clathrate crystallographic structure was refined assuming a cubic lattice (space group $P4_132$, No. 213) of type-III clathrate published previously (Fig. 1), i.e., Si(1) at 8*c* (x,x,x) with $x = 0.0362$, Si(2) at 24*e* (0.2038,0.0427,0.0001), Si(3) at 12*d* $(1/8,y,y+1/4)$ with $y = 0.1696$, Si(4) at 24*e* (0.2387,0.9394,0.8752), Si(5) at 24*e* (0.4156,0.8605,0.0769), Si(6) at 8*c* (x,x,x) with $x = 0.3256$, Ba(1) at 8*c* (x,x,x) with $x = 0.1887$ in the small Si_{20} cages, Ba(2) at 4*b* (7/8,7/8,7/8) in cubic Si_8 cages, and Ba(3) at 12*d* $(1/8,y,y+1/4)$ with $y = 0.8072$ in the distorted $Si_{20}(\text{vacancy})_4$ cages. During the refinement of the XRD patterns the 14 structural parameters of the nine Wyckoff sites (three barium and six silicon sites) of $Ba_{24}Si_{100}$ were refined. All the Debye-Waller factors of the atoms were chosen as being isotropic.

In Fig. 3 we present the observed, calculated, and difference curves of the $Ba_{24}Si_{100}$ XRD pattern at ambient pressure (in the DAC) after Rietveld refinement; there is good agreement between the experimental and the calculated profiles. The low pressure Si (diamond structure) and cubic $BaSi_2$ minority phases were taken into account, but only their scale factor, lattice parameter, and profile shape parameters were refined. The calculated fractions of impurities were 3.9(6)% (Si) and 2.3(6)% ($BaSi_2$) in weight from the Rietveld refinement. The successive phase transitions of silicon in a β-tin-type phase at 11–12 GPa, then in a hexagonal Si-V phase at 15–16 GPa, were taken into account (see the inset of Fig. 3 where $Ba_{24}Si_{100}$ and Si-V phases were taken into account in the Rietveld refinement of the XRD pattern acquired at 23.45 GPa).

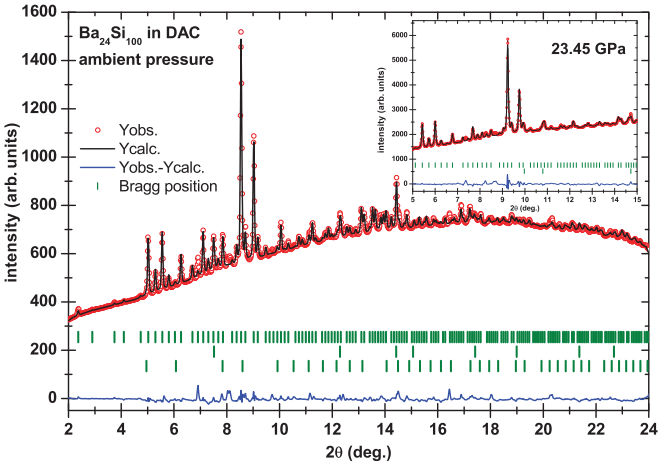

FIG. 3. (Color online) Rietveld refinement ($\lambda = 0.4108$ Å) of our $Ba_{24}Si_{100}$ powder sample (loaded in the DAC) at ambient pressure and room temperature and at 23.45 GPa (inset). A difference curve is plotted at the bottom (observed minus calculated intensities). Tick marks correspond to Bragg peaks of the clathrate phase (first row) and impurities: Si diamond (second row) and $BaSi_2$ (third row). In the inset the first row of marks correspond to $Ba_{24}Si_{100}$ and the second row to the Si-V high pressure phase of silicon.

C. Pressure-induced evolution in $Ba_{24}Si_{100}$

1. *Phase transitions and bulk modulus*

Figure 4 shows some XRD patterns during compression of the sample up to 37.4 GPa (upper part) and during pressure release (lower part). All the Bragg peaks shift to larger angles, showing the shrinkage of the cubic $Ba_{24}Si_{100}$ lattice. In particular, the XRD pattern of our sample is still present above 23 GPa, and despite the broadening of the peaks

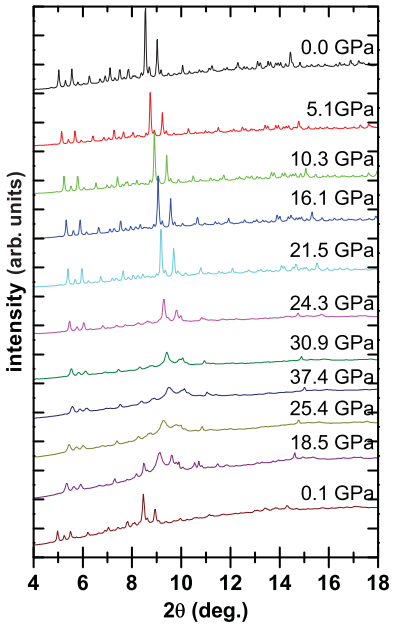

FIG. 4. (Color online) XRD patterns of $Ba_{24}Si_{100}$ ($\lambda = 0.4108$ Å) during the pressurization from ambient conditions to 37.4 GPa and decompression down to the full release of pressure (from top to bottom).

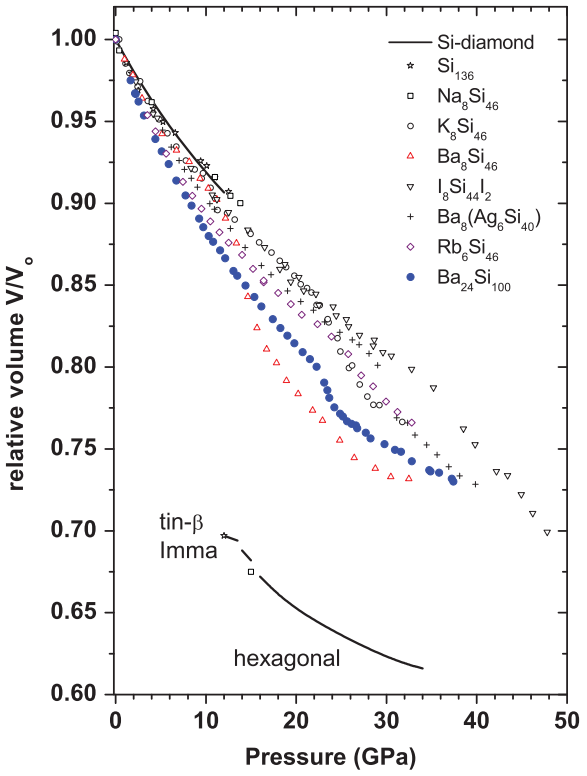

FIG. 5. (Color online) Variation of the relative volume of $Ba_{24}Si_{100}$ type-III clathrate vs pressure compared with other silicon type-I M_8Si_{46} (M = Na, K, Rb, Ba, I) and type-II Si_{136} clathrates.

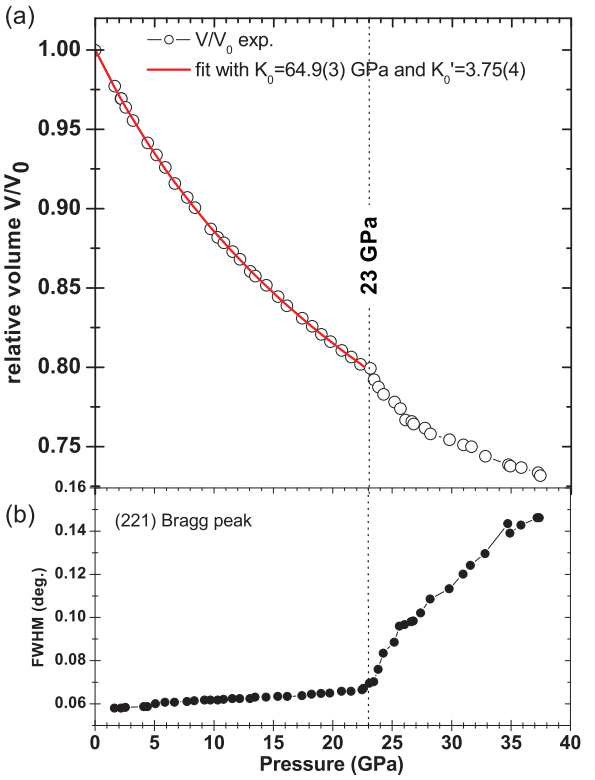

FIG. 6. (Color online) (a) Experimental relative volume of $Ba_{24}Si_{100}$ lattice vs pressure; two different fits are also plotted (see text). (b) Full width at half maximum (FWHM) of the (221) Bragg peak of $Ba_{24}Si_{100}$ as a function of pressure.

the pattern remains qualitatively the same than the one at ambient pressure. Remarkably enough, we keep observing XRD crystalline-type patterns above 23 GPa, i.e., beyond the pressure where Shimizu *et al.* observed the complete attenuation of all the Raman peaks of $Ba_{24}Si_{100}$.[10]

As illustrated in Figs. 5 and 6(a) (variation of the relative volume of the lattice), the $Ba_{24}Si_{100}$ lattice parameter decreases continuously with pressure, reaching 13.04(1) Å at 23 GPa. At this pressure the relative volume of the lattice is 80% of the initial one (i.e., a reduction of 20% of the cubic lattice). Above this point, the reduction of the relative volume changes its regime, as shown by the kink in the V/V_0 curve as a function of pressure ~23 GPa (Fig. 5). This behavior of the relative volume is very similar to the one in type-I silicon clathrates M_8Si_{46} (M = Ba, Sr, Rb, K, Na, I), the kink in the relative volume curve being the signature of the volume collapse of the lattice. At this point, we notice that $Ba_{24}Si_{100}$ has a higher volume collapse pressure than the ones in Na_8Si_{46} or Ba_8Si_{46} (13–15 GPa) and in the nonintercalated Si_{136} clathrate (10–11 GPa). The volume collapse pressure of our type-III clathrate exhibits a value much closer to the case of K_8Si_{46} (20–26 GPa) or $Rb_{6.15}Si_{46}$ (23–25 GPa) (see Fig. 5 and Table I). However, this value remains lower than the pressure for which the collapse is observed in $I_8(Si_{44}I_2)$ or $Ba_8(Ag_{46}Si_{40})$ (~35 and 28 GPa, respectively), i.e., a compound with initial lattice parameters higher than the ones of the Ag unsubstituted compound. Increasing the size of the silicon cages and conserving the same guest atoms in the cages appears then to push the lattice collapse to higher pressures.

This relationship between the size of the host network and the pressure instabilities was also recently evidenced in Ge-based clathrates by Kume *et al.*[29] In addition, in $Ba_8(Ga_{16}Ge_{30})$, these authors have demonstrated that before the volume collapse the displacement of host atoms in the Wyckoff 24*k* position during the compression of the clathrate gives rise to the deformation of the hexagonal ring in the large $(Ga,Ge)_{24}$ cage. In $Ba_{24}Si_{100}$, the absence of four Si atoms forming these hexagonal rings in the normal Si_{24} cages (replaced by Si_{24} cages with four vacancies) then could be at the origin of its higher volume collapse pressure. We will discuss the internal structure changes in more detail later in the article.

TABLE I. Pressures of volume collapse and amorphization for type-III $Ba_{24}Si_{100}$ as compared to other type-I M_8Si_{46} and type-II M_xSi_{136} clathrates. See also Fig. 5.

Compound	$P_{collapse}$ (GPa)	$P_{amorphization}$ (GPa)	Ref.
$Ba_{24}Si_{100}$	23.0(5)	>37 GPa	This work
Ba_8Si_{46}	14(1)	40(3)	14
$Ba_8(Ag_6Si_{40})$	28(3)	>40 GPa	Our work[a]
$Rb_{6.15}Si_{46}$	24(1)	33(1)	18
K_8Si_{46}	23(3)	32(3)	16
Na_8Si_{46}	13(2)	–	14
$I_8(Si_{44}I_2)$	35(3)	47(3)	14
Na_1Si_{136}	11(1)	–	12,22

[a]Unpublished.

In Fig. 6(a), our V/V_0 $Ba_{24}Si_{100}$ data points upon compression in the low pressure range 0–22.5 GPa were fitted using a Murnaghan equation-of-state model to obtain the bulk modulus K_0 and its pressure derivative K_0'. The values obtained by this procedure are $K_0 = 64.9(3)$ GPa and $K_0' = 3.75(4)$; this value of K_0' is very close to the ones usually found for other type-I and type-II Si clathrates by San-Miguel *et al.*[12] (3.6, a value obtained by a Murnaghan fitting analysis of theoretical calculated data points for Si_{136}) and for Si-diamond [3.8(4) (Ref. 30)].

We have also used an alternative fitting procedure based on the normalized or reduced stress-strain variables F and f.[31,32] The Eulerian strain parameter f and the normalized pressure F are defined as follows: $f = 1/2[(V/V_0)^{-2/3} - 1]$ and $F = P[3f(1+2f)^{2.5}]^{-1}$. This formalism yields the second-order finite strain equation $F = K_0[1 - 1.5(4 - K_0')f]$. As shown in Fig. 7, in the different pressure regions, in particular, below 23 GPa i.e., before the volume collapse, the F-f plot is in fact a straight line, and from its intercept as f goes to zero and its slope, we obtain $K_0 = 65.0(3)$ GPa and $K_0' = 3.90(6)$. This is in agreement with the values obtained with our previous approach. To summarize, $Ba_{24}Si_{100}$ shows a bulk modulus of $K_0 = 65.0(4)$ GPa with $K_0' = 3.8(1)$, in that sense it is more compressible than other inorganic Si-based clathrates. This is particulary visible in Fig. 5 (see also Table II, which summarizes also the data available in the literature for different types of silicon clathrates), where one can see that the relative volume of the type-III silicon $Ba_{24}Si_{100}$ clathrate decreases faster with pressure (before the HVC) than the other type-I M_8Si_{46} or type-II M_xSi_{136}. It seems that a general trend in clathrates formed of Si_{20} and Si_{24} cages (types I and III) is that when all the silicon cages are filled at their maximal content, the bulk modulus of the corresponding clathrates are in the range of 85–95 GPa; if one type of cage is quasiempty

TABLE II. Bulk modulus K_0 and its derivative K_0' for type-III $Ba_{24}Si_{100}$ and other type-I M_8Si_{46} and type-II M_xSi_{136} clathrates.

Compound	K_0 (GPa)	K_0'	Ref.
$Ba_{24}Si_{100}$	65.0(4)	3.8(1)	This work
Ba_8Si_{46}	93 ± 5	3.6	14
$Rb_{6.15}Si_{46}$	78(1)	3.6	18
$Rb_{6.15}Si_{46}$ (from F-f plot)	61.4(7)	6.7(2)	18
K_8Si_{46}	86 ± 5	?	16
Na_8Si_{46}	94 (calc.)	–	14
$I_8(Si_{44}I_2)$	95 ± 5	3.6	14
Na_1Si_{136}	90 ± 5	3.6	12

(the case of $Rb_{6.15}Si_{46}$) this bulk modulus drops to a lower value (78 GPa); and finally when a part of the atoms forming the cages are absent (as in our present $Ba_{24}Si_{100}$ compound), the silicon network is less strong to sustain the external pressure and more compressible, and as a consequence the bulk modulus decreases again to 65 GPa.

2. *Evolution of the internal structural parameters*

The XRD patterns were fitted by Rietveld refinement up to 25 GPa. As mentioned before, the atomic positions were refined, keeping the isotropic thermal factors (Biso) constant (at their initial values refined at room pressure) and refining the profile parameters of the peaks. In a second refinement protocol, the Biso were simultaneously fitted with the internal atomic positions and other parameters (peak profile and lattice parameters). Both approaches give the same result, represented in Fig. 8: The relative positions of the atoms inside the lattice do not change up to the volume collapse at 23 GPa. We note that the transition seen by Raman spectroscopy[10] between 3.9 and 6.5 GPa is not detected here. Between 23 and 25 GPa, i.e., at the beginning of the volume collapse, it

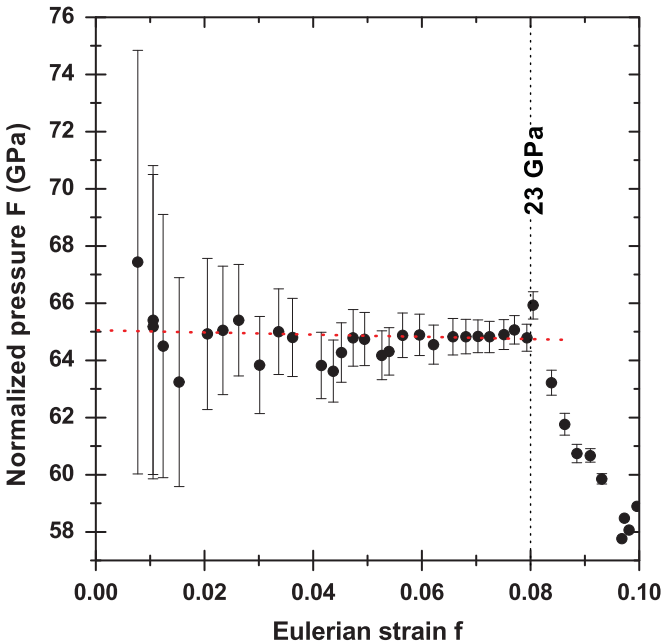

FIG. 7. (Color online) Normalized pressure (F) as a function of the Eulerian strain (f) induced in the lattice of $Ba_{24}Si_{100}$ under pressure.

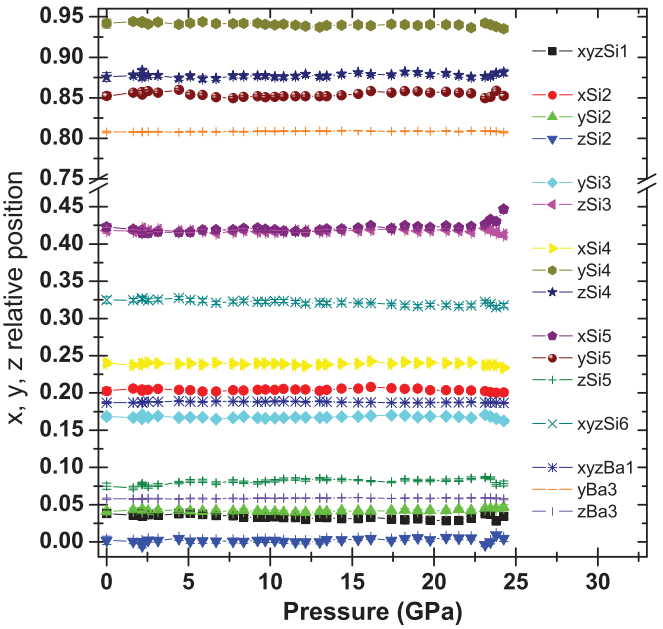

FIG. 8. (Color online) Relative position of the atoms in the $Ba_{24}Si_{100}$ lattice as a function of pressure, obtained from Rietveld refinement. Error bars are smaller than the size of the symbols.

seems that some Si atoms start to move slightly from their relative position Si(3) [common in Si_{20} and Si_{20}(vacancy)$_4$ cages] and Si(5) [common in the three types of cages; for example, see Fig. 1], while the average positions of the three Ba sites is not affected. This is the sign that some disorder starts to appear in the silicon-host network. As a consequence, the average Si-Si distances are changed, and some of them are strongly renormalized. This is the case of the ones around the central Si_5 atom, common in three kinds of cages, for example, the Si(1)-Si(5) distance [i.e., the one common in pseudocubic Si_8 and Si_{20}(vacancy)$_4$ cages] which increases from 3.85(4) Å at 22.3 GPa to 4.28(5) Å at 24.8 GPa (i.e., a change of 11%). We remark that before the collapse all the Si nanocages are deformed isostructurally, with all the distances decreasing at the same rate. This case is different from the case of the Ge/Ga-based clathrate $Ba_8(Ga_{16}Ge_{30})$ studied by Kume *et al.*,[29,34] where the relative position of the Ge/Ga 24*k* site changes with pressure (while the other sites stay at the same relative position) before the lattice collapse; this movement of the 24*k* site is certainly related to the volume collapse in this Ga/Ge type-I clathrate. At this point we cannot make a direct relationship between the lowest-energy Raman mode and the average guest-host distance, which was proposed by the previous cited work of Kume *et al.* to evidence the collapse critical point, characterized by the softening of the low-energy phonon. Nevertheless, the work of Shimizu *et al.*[10] show that the 48 cm^{-1} mode of $Ba_{24}Si_{100}$, related to the Ba(3) large Si_{20}(vacancy)$_4$ cage, hardens at the beginning of the compression, then flattens at ∼20 GPa, and seems to soften just below the onset of the volume collapse. Another key parameter related to the lattice collapse can be the mode of the Ba(2) encaged in the pseudocubic Si_8. These issues are certainly interesting to investigate in more detail to determine if a critical behavior of one of the low-energy phonons of $Ba_{24}Si_{100}$ are at the origin of its volume collapse.

Above 25 GPa, the refinement is unstable and diverges, probably because it becomes impossible to modelize the structure using the initial structural model, the disorder of the structure being too strong.

Figure 9 shows the variation of the refined values of isotropic thermal factors obtained from the Rietveld refinement. The one from the silicon atoms (taken to be identical for all Si atoms) does not show a large variation up to the volume collapse at 23 GPa. In contrast, the variation in the three thermal factors of Ba atoms shows three distinguishable regimes: Below 5 GPa, they decrease moderately, then they increase discontinuously to the second regime, where Biso of Ba_2 (in cubic Si_8 cages) and Ba_3 (in Si_{24} cages with four vacancies) decrease again slowly with pressure while the one of Ba_1 (in regular Si_{20} cages) stays constant up to 23 GPa. This change in the thermal factors of Ba atoms at 5 GPa is not an artifact due to the nitrogen freezing because nitrogen solidifies at ∼2.4 GPa (at room temperature).[33] Moreover, this result is consistent with the general decrease of the intensity of the modes associated with the vibrations of Ba atoms measured by Raman spectroscopy between 3.9 and 6.5 GPa.[10] This is also a proof that the nature of the transmitting medium (argon in the Raman spectroscopy study and nitrogen here) does not influence the transition observed here.

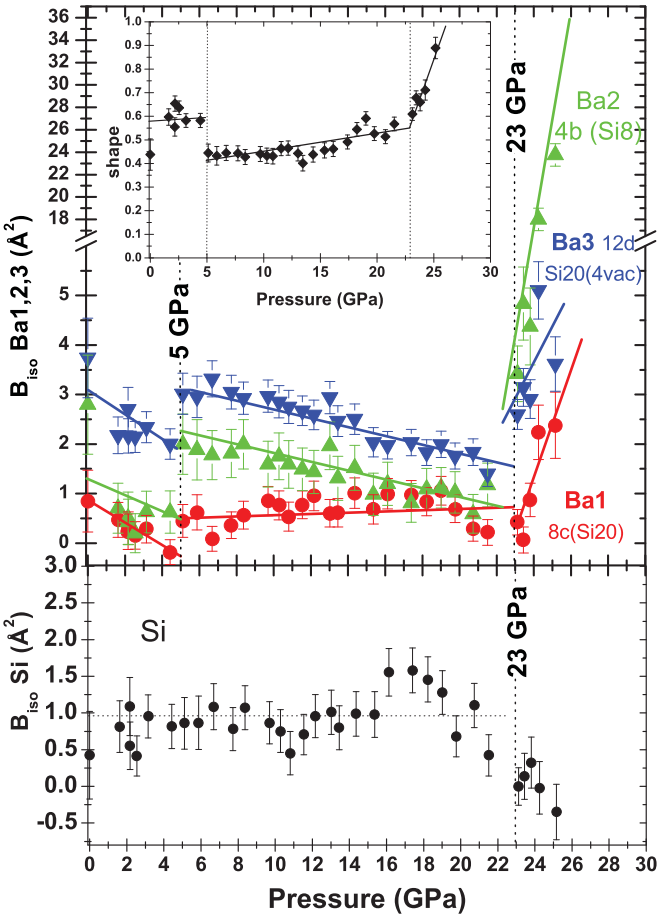

FIG. 9. (Color online) Isotropic thermal factors of Ba(1, 2, and 3) atoms (top panel) and Si atoms (all sites constrained to the same value) (bottom panel) of $Ba_{24}Si_{100}$ as a function of pressure, obtained from Rietveld refinement. Inset of top panel: Variation of the shape parameter of the $Ba_{24}Si_{100}$ Bragg peaks (ratio between the Gaussian and Lorentzian contributions) with pressure.

Finally, between 23 and 25 GPa, i.e., in the first stage of the volume collapse, all the three Ba Biso increase hugely, in particular, the one of Ba_2 (atom in large cubic Si_8 cage) reaching very large values; this site of Ba_2 is the most affected by the volume collapse and the large values attained (unphysical) of Biso are a sign of a strongly disordered site.

The two transitions are also marked in the variation of the shape parameter of the peak profile (i.e., the ratio between the Gaussian and Lorentzian contributions) which has a step toward a lower value at 5 GPa followed by a slow increase with pressure, reflecting the continuous broadening of the Bragg peaks, and finally a second transition at 23 GPa toward a faster regime when the lattice collapses. Again, the transition pressures are coherent with the previous high pressure Raman spectroscopy study.[10]

3. *Above the volume collapse at 23 GPa*

As described before, at 23 GPa the $Ba_{24}Si_{100}$ lattice collapses, as shown by the kink in the curve of its relative volume, a sign of the sudden change in compressibility of the material [Figs. 5 and 6(a)]. The change in compressibility before and after 23 GPa is also clearly visible on the

F-f plot (Fig. 7), which shows a discontinuity at $f = 0.08$, corresponding to $P = 23$ GPa.

No halo is found on the XRD images above the volume collapse at 23 GPa, which is a usual sign of amorphization, as observed for instance above 33 GPa in $Rb_{6.15}Si_{46}$.[18] Moreover, at the highest pressure reached, 37.4 GPa, we still have diffraction peaks with no significant change of the relative intensities. The amorphization pressure in this type-III clathrate is then at least higher than the ones of $Rb_{6.15}Si_{46}$ and K_8Si_{46}, ∼32–33 GPa (see Table I) and finally of the same order than other Si-based type-I clathrates.

However, at very high pressure, we observe a broadening, as shown in Fig. 6(b) for the (221) Bragg peak (∼5° at ambient pressure), all the diffraction peaks become quickly broader above 23 GPa; this is the case also for the most intense (431) and (520) reflections.

As mentioned in the previous section, it was not possible to refine the atomic positions at such high pressure, but the important point is that we do observe a diffraction signal at 37.4 GPa while the typical Raman spectrum of $Ba_{24}Si_{100}$ is fully lost at 23.2 GPa. This situation has also been observed in $Sr_8(Ga_{16}Ge_{30})$, $Ba_8(Ga_{16}Ge_{30})$,[29,34] and $I_8(Sb_8Ge_{38})$,[35] where XRD peaks are still present even when the characteristic Raman spectra of the clathrate structure are lost. All these observations suggest that, in $Ba_{24}Si_{100}$, above 23 GPa, the average clathrate structure even if preserved, it is probably highly distorted. This may lead to a change of selection rules and result in spread and weak Raman signal similar to the one of an amorphous structure.

Concerning this point, the case of the germanium-based $Ba_{24}Ge_{100}$ clathrate could be analogous to the one of $Ba_{24}Si_{100}$. In fact, Shimizu *et al.*[8] found in a Raman study the amorphization of $Ba_{24}Ge_{100}$ at pressures above 22 GPa based on similar arguments for $Ba_{24}Si_{100}$. It should be then worth considering that the observed transition at 22 GPa could correspond to a volume collapse associated to a distorted-cage clathrate phase, as for $Ba_{24}Si_{100}$. Further studies (XRD under HP, for example) are needed.

A second point is illustrated in Fig. 10, where it is compared the XRD pattern of our $Ba_{24}Si_{100}$ powder in the DAC before compression and after an excursion at 37.2 GPa, at nearly zero pressure (after pressure release). The XRD patterns are identical (the peaks are slightly broader because of defaults created during the compression) proving that the transition at 23 GPa is quasireversible. The comparison shows also that the Bragg peaks are at a slightly lower angle after compression, i.e., the clathrate lattice has expanded a little bit after this high pressure excursion. It is probably due to the fact that the cage distortions induced above 22 GPa are not completely released even after pressure release.

Our interpretation of all these results is that the silicon network remains ordered in the initial structure up to the volume collapse. Then, at the volume collapse, a strong disorder appears in all the Si sites leading to the annihilation of the Raman-active modes. The nanocage architecture is nevertheless maintained and no amorphization is reached. In fact, even at 37.4 GPa (broad) Bragg peaks still exist, and after full decompression,(nearly) the same initial XRD pattern can be recovered. This last fact points to the formation of a

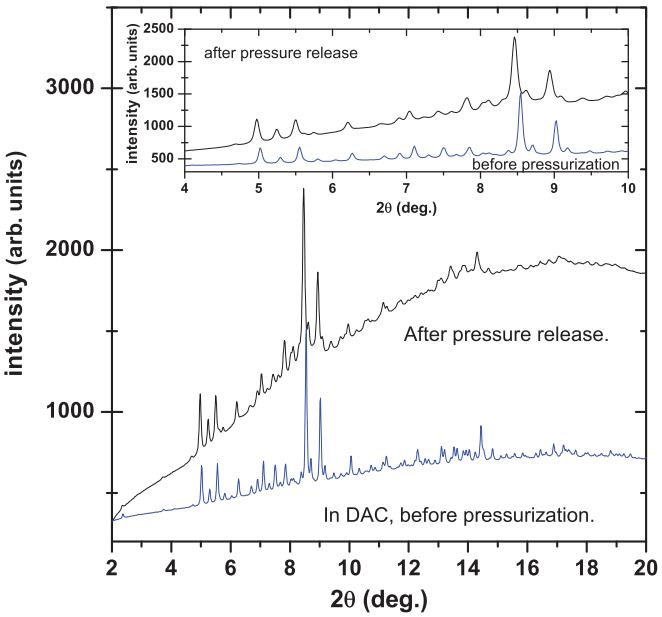

FIG. 10. (Color online) XRD patterns ($\lambda = 0.4108$ Å) of the $Ba_{24}Si_{100}$ sample before (at ambient conditions, in DAC) and after the pressure run (up to 37 GPa). Inset: 4°–10° 2θ range view.

nanocage-based disordered structure after the volume collapse which, on pressure release, reverses toward the initial ordered structure (at least up to 37.4 GPa). The volume collapse occurring at 23 GPa is then reversible.

Finally, let us consider the first transition at 5 GPa, evidenced by Raman spectroscopy[10] and in our study. Our data shows that it is related to the Ba atoms which show a step to a larger amplitude of their oscillation above 5 GPa. This could be the sign of an off-centering (dynamic or static) of the Ba positions relatively to the center of the Si cages. From our data, we cannot conclude if some Ba sites are split in different static sites with a hopping between them or not, because their average positions stay the same across the transition at 5 GPa. Nevertheless, if this splitting exists, it should remain small and probably undetectable by powder diffraction.

IV. CONCLUSION

The silicon type-III clathrate $Ba_{24}Si_{100}$ has been studied by powder x-ray diffraction at high pressure using a diamond anvil cell and nitrogen as a pressure-transmitting medium. It is found that $Ba_{24}Si_{100}$ has a smaller bulk modulus [with $K_0 = 65.0(4)$ GPa] than the other Si-based clathrates, with similar K_0' [3.8(1)].

In agreement with the previous high pressure study of Shimizu *et al.* using Raman spectroscopy,[10] two transitions are found, at 5 and 23 GPa, but our interpretation for the second one differs from the one proposed by Shimizu *et al.* Similar to type-I silicon clathrates M_8Si_{46}, $Ba_{24}Si_{100}$ undergoes a volume collapse which is observed at ∼23 GPa, a value higher than for Ba_8Si_{46} (13–15 GPa) which is built from the same Si_{20} cages but with full Si_{24} cages, whereas $Ba_{24}Si_{100}$ has four silicon vacancies on its Si_{24} cages. The presence of these vacancies and of a third barium site in a cubic Si_8 cage might be the

origin of its lower bulk modulus but higher stability before the volume collapse.

In the lower pressure phase transition, the Si network is not affected, but the Ba atoms show a pronounced discontinuous positive variation of their isotropic thermal factors, which we interpret as a sign of random disordering of the encaged atoms with an associated change of their hybridization with the Si network. Then, at the second transition at 23 GPa, the host network and guest atoms are more strongly affected, probably with the creation of a very distorted and disordered structure. This disordered but nanocage-based structure explains why Shimizu *et al.* observed the full disappearance of the Raman modes of $Ba_{24}Si_{100}$. This form of disorder for pressures above 23 GPa cannot be considered as an amorphization, as proved by the observation of the typical XRD pattern of $Ba_{24}Si_{100}$ (with very broad Bragg peaks) up to 37.4 GPa. Moreover, the collapse of the lattice at 23 GPa is reversible at least up to 37.4 GPa.

*Corresponding author: pierre.toulemonde@grenoble.cnrs.fr

[1] J. S. Kasper, P. Hagenmuller, M. Pouchard, and C. Cros, Science **150**, 1713 (1965).
[2] C. Cros, M. Pouchard, and P. Hagenmuller, J. Solid State Chem. **2**, 570 (1970).
[3] A. San-Miguel and P. Toulemonde, High Press. Res. **25**, 159 (2005).
[4] S. Yamanaka, Dalton Trans. **39**, 1901 (2010).
[5] F. M. Grosche, H. Q. Yuan, W. Carrillo-Cabrera, S. Paschen, C. Langhammer, F. Kromer, G. Sparn, M. Baenitz, Yu. Grin, and F. Steglich, Phys. Rev. Lett. **87**, 247003 (2001).
[6] H. Q. Yuan, F. M. Grosche, W. Carrillo-Cabrera, S. Paschen, G. Sparn, M. Baenitz, Yu. Grin, and F. Steglich, J. Phys. Condens. Matter **14**, 11249 (2002).
[7] H. Q. Yuan, F. M. Grosche, W. Carrillo-Cabrera, V. Pacheco, G. Sparn, M. Baenitz, U. Schwarz, Yu. Grin, and F. Steglich, Phys. Rev. B **70**, 174512 (2004).
[8] H. Shimizu *et al.*, J. Appl. Phys. **101**, 113531 (2007).
[9] T. Rachi *et al.*, Phys. Rev. B **72**, 144504 (2005).
[10] H. Shimizu, T. Kume, T. Kuroda, S. Sasaki, H. Fukuoka, and S. Yamanaka, Phys. Rev. B **71**, 094108 (2005).
[11] S. Yamanaka, E. Enishi, H. Fukuoka, and M. Yasukawa, Inorg. Chem. **39**, 56 (2000).
[12] A. San-Miguel, P. Kéghélian, X. Blase, P. Mélinon, A. Perez, J. P. Itié, A. Polian, E. Reny, C. Cros, and M. Pouchard, Phys. Rev. Lett. **83**, 5290 (1999).
[13] T. Kume, H. Fukuoka, T. Koda, S. Sasaki, H. Shimizu, and S. Yamanaka, Phys. Rev. Lett. **90**, 155503 (2003).
[14] A. San Miguel, P. Mélinon, D. Connétable, X. Blase, F. Tournus, E. Reny, S. Yamanaka, and J. P. Itié, Phys. Rev. B **65**, 054109 (2002).
[15] A. San Miguel, A. Merlen, P. Toulemonde, T. Kume, S. Le Floch, A. Aouizerat, S. Pascarelli, G. Aquilanti, O. Mathon, T. Le Bihan, J. P. Itié, and S. Yamanaka, Europhys. Lett. **69**, 556 (2005).
[16] J. S. Tse, S. Desgreniers, Z. Q. Li, M. R. Ferguson, and Y. Kawazoe, Phys. Rev. Lett. **89**, 195507 (2002).
[17] T. Kume, T. Koda, S. Sasaki, H. Shimizu, and J. S. Tse, Phys. Rev. B **70**, 052101 (2004).
[18] D. Machon, P. Toulemonde, P. F. McMillan, M. Amboage, A. Munoz, P. Rodriguez-Hernandez, and A. San Miguel, Phys. Rev. B **79**, 184101 (2009).
[19] P. Toulemonde, Ch. Adessi, X. Blase, A. San-Miguel, and J. L. Tholence, Phys. Rev. B **71**, 094504 (2005).
[20] P. Toulemonde, A. San-Miguel, A. Merlen, R. Viennois, S. Le Floch, Ch. Adessi, X. Blase, and J. L. Tholence, J. Phys. Chem. Sol. **67**, 1117 (2006).
[21] H. Shimizu, T. Kume, T. Kuroda, S. Sasaki, H. Fukuoka, and S. Yamanaka, Phys. Rev. B **68**, 212102 (2003).
[22] G. K. Ramachandran, P. F. McMillan, S. K. Deb, M. Somayazulu, J. Gryko, J. Dong, and O. F Sankey, J. Phys. Condens. Matter **12**, 4013 (2000).
[23] H. Fukuoka, K. Ueno, and S. Yamanaka, J. Organomet. Chem. **611**, 543 (2000).
[24] R. Viennois, P. Toulemonde, C. Paulsen, and A. San-Miguel, J. Phys. Condens. Matter **17**, L311 (2005).
[25] J. S. Tse, R. Flacau, S. Desgreniers, T. Iitaka, and J. Z. Jiang, Phys. Rev. B **76**, 174109 (2007).
[26] E. Reny, A. San-Miguel, Y. Guyot, B. Masenelli, P. Mélinon, L. Saviot, S. Yamanaka, B. Champagnon, C. Cros, M. Pouchard, M. Borowski, and A. J. Dianoux, Phys. Rev. B **66**, 014532 (2002).
[27] A. P. Hammersley, S. O. Svensson, M. Hanfland, A. N. Fitch, and D. Häusermann, High Press. Res. **14**, 235 (1996).
[28] J. Rodríguez-Carvajal, Physica B **192**, 55 (1993).
[29] T. Kume, S. Ohno, S. Sasaki, H. Shimizu, Y. Ohishi, N. L. Okamoto, K. Kishida, K. Tanaka, and H. Inui, J. Appl. Phys. **107**, 013517 (2010).
[30] M. I. McMahon, R. J. Nelmes, N. G. Wright, and D. R. Allan, Phys. Rev. B **50**, 739 (1994).
[31] R. Jeanloz and R. M. Hazen, Am. Mineral. **76**, 1765 (1991).
[32] R. J. Angel, in *High-Pressure, High-Temperature Crystal Chemistry*, edited by R. M. Hazen and R. T. Downs, Reviews in Mineralogy and Geochemistry (Mineralogical Society of America and the Geochemical Society, Washington, DC, 2000), Vol. 41, pp. 35–60.
[33] R. J. Angel, M. Bujak, J. Zhao, G. D. Gatta, and S. D. Jacobsen, J. Appl. Crystallogr. **40**, 26 (2007).
[34] T. Kume, S. Sasaki, and H. Shimizu, Phys. Chem. Solids **71**, 583 (2010).
[35] H. Shimizu, R. Oe, S. Ohno, T. Kume, S. Sasaki, K. Kishimoto, T. Koyanagi, and Y. Ohishi, J. Appl. Phys. **105**, 043522 (2009).